Transcription factor bHLH121 regulates root cortical aerenchyma formation in maize

Hannah M. Schneider[a,b,1], Vai S. Lor[c,1], Xia Zhang[c,d], Patompong Saengwilai[a,e], Meredith T. Hanlon[a], Stephanie P. Klein[a] (ID), Jayne L. Davis[f] (ID), Aditi N. Borkar[g] (ID), Cody L. Depew[a], Malcolm J. Bennett[f] (ID), Shawn M. Kaeppler[c,d] (ID), Kathleen M. Brown[a] (ID), Rahul Bhosale[f] (ID), and Jonathan P. Lynch[a,2] (ID)

Root anatomical phenotypes present a promising yet underexploited avenue to deliver major improvements in yield and climate resilience of crops by improving water and nutrient uptake. For instance, the formation of root cortical aerenchyma (RCA) significantly increases soil exploration and resource capture by reducing the metabolic costs of root tissue. A key bottleneck in studying such phenotypes has been the lack of robust high-throughput anatomical phenotyping platforms. We exploited a phenotyping approach based on laser ablation tomography, termed *Anatomics*, to quantify variation in RCA formation of 436 diverse maize lines in the field. Results revealed a significant and heritable variation for RCA formation. Genome-wide association studies identified a single-nucleotide polymorphism mapping to a root cortex-expressed gene-encoding transcription factor bHLH121. Functional studies identified that the *bHLH121* Mu transposon mutant line and CRISPR/Cas9 loss-of-function mutant line showed reduced RCA formation, whereas an overexpression line exhibited significantly greater RCA formation when compared to the wild-type line. Characterization of these lines under suboptimal water and nitrogen availability in multiple soil environments revealed that *bHLH121* is required for RCA formation developmentally as well as under studied abiotic stress. Overall functional validation of the *bHLH121* gene's importance in RCA formation provides a functional marker to select varieties with improved soil exploration and thus yield under suboptimal conditions.

aerenchyma | anatomy | maize | root | cortex

Significance

Root anatomical phenotypes are important for soil resource acquisition, particularly in stressful environments. Using *Anatomics* (anatomical phenotyping) coupled with GWAS, we identified and then validated a bHLH transcription factor that regulates the formation of root cortical aerenchyma, an important phenotype for water and nutrient acquisition. Understanding the genetic regulation of root anatomical phenotypes promises to accelerate the breeding of crop cultivars with improved stress tolerance, resilience, and carbon sequestration.

Improvements in the yield of cereal crops such as wheat and maize have recently plateaued (1). This is a major cause for concern with respect to food security, particularly given projected global population growth and the impact of climate change on crop productivity. In high-input agricultural systems, intensive fertilization and irrigation cause massive environmental degradation and are not sustainable, while in the low-input agriculture characteristic of developing nations, limited availability of water and nutrients are primary limitations to crop production, food security, and economic development (2–4). Therefore, crops and cropping systems with greater resource efficiency and climate resilience are urgently needed in global agriculture.

Understanding the genetic architecture of root traits (or phenes where "phene" is to "phenotype" as "gene" is to "genotype") (5–7) is an important aid in ideotype or trait-based crop improvement (8, 9). For edaphic stress, root anatomical phenotypes play important roles in soil resource capture as they determine the spatiotemporal distribution of root foraging in distinct soil domains and thus the capture of immobile and mobile soil resources (4, 8, 10–14). Root anatomical phenotypes have the potential to deliver major improvements in crop production by improving resource capture, transport, and utilization (4, 15–17). Several root anatomical phenotypes reduce carbon and nutrient costs of tissue construction and maintenance, thereby improving the metabolic efficiency of soil exploration, and thereby plant growth and yield, particularly in edaphic stress (4, 8, 14, 16, 17). Reduced cortical cell file number and increased cortical cell size reduce root respiration and increase rooting depth, leading to improved water acquisition and greater yield under drought (18, 19). Root cortical senescence (i.e., programmed cell death (PCD) of the entire root cortex) in temperate small grains (e.g., barley, wheat) enables greater exploration of deeper soil domains and greater plant growth in edaphic stress due to reduced cortical burden (20–22). In dicots, reduced secondary growth results in less root respiration and subsequently greater root length, nutrient capture, and plant growth in low phosphorus soil (23).

Formation of root cortical aerenchyma (RCA), which converts living cortical cells to air space via PCD (24), also improves crop growth and productivity under suboptimal water

and nutrient availability (15, 25–29). Living cortical parenchyma are replaced with air-filled lacunae, reducing root respiration and nutrient demand (27–29). In roots with RCA, reduced nutrient and carbon demand associated with tissue maintenance costs enable greater soil exploration, greater capture of water, nitrogen, phosphorus, and potassium, and greater plant growth and yield in dry and infertile soils (4, 15, 16, 25–30). RCA represents a promising target for crop breeding.

Despite this knowledge, RCA and other anatomical phenotypes have received little attention as selection criteria in plant breeding because of the challenges of sampling root systems from soil and quantifying anatomical phenotypes. This challenge is magnified in genetic studies due to the numbers of accessions that must be evaluated. To date, studies of root anatomical phenotypes are usually limited to artificial growth environments, limited genotypes, and few replications due to difficulties in obtaining and analyzing root cross-sectional images from a large number of samples (e.g., ref. 30). Greenhouse-based studies have identified quantitative trait loci (QTL) for RCA in *Zea* species (31, 32) and in maize (33). In addition, genetic loci have been identified for the expression of RCA in maize in well-watered and water-stressed environments and their plastic response to water deficit in the field (34).

In this study, we used *Anatomics* (an anatomical phenotyping pipeline involving *shovelomics* [36] in combination with Laser Ablation Tomography (LAT) imaging and data quantification using *RootScan* image analysis software) to phenotype field grown mature plants of a maize diversity panel for root anatomy to identify genes controlling variation in RCA (35–39). The Wisconsin Diversity Panel has been genotyped with a high marker density and has very small linkage blocks, allowing for precise detection of candidate genes and the identification of rare alleles. We used Genome-wide association studies (GWAS) to identify a candidate gene controlling RCA in maize. We validated the regulatory role of the candidate gene *ZmbHLH121* in RCA formation through a transposon insertion mutant, overexpression, and CRISPR-Cas9 gene-edited lines.

Results

### GWAS Reveal *ZmbHLH121* Is Associated with RCA Formation.
RCA formation was phenotyped using the *Anatomics* pipeline on 436 field-grown maize inbred lines from the Wisconsin Diversity Panel (Fig. 1) (34). We observed striking variation in RCA formation with values ranging from 0 to 41% of the total cortical cross-sectional area. RCA formation was relatively heritable (H^2 = 0.59). Our GWAS identified two significant single-nucleotide polymorphisms (SNPs) (SNP_191380766 and SNP_191380613) located in the 5′UTR (untranslated region) of the gene model *Zm00001d006065* (LOC100383077, located on chromosome 2 at position 197129772) (Fig. 1). The 5′ UTR region is known to have various regulatory elements (transcription factor (TF)-binding sites, cis-regulatory elements, and trans-regulatory factors e.g., RNA-binding proteins) and plays a major role in the control of translation initiation. We checked whether there are any TF-binding sites present at the GWAS-identified SNP positions and whether the polymorphism changes/mutates any of those sites. In the 5′ reference sequence there are five TF-binding sites of interest. Three are ethylene response factors bound by 3 separate three TFs. Two are lateral organ boundaries domain sites bound by a single TF. Mutating the nucleotide at 19713367 from the reference identity, G, to T results in the disappearance of these sites. As ethylene is known to induce RCA formation; the GWAS-identified SNPs that are present in the UTR region of *bHLH121* may be involved in modulating the RCA phenotype through ethylene-induced PCD.

In addition to GWAS-identified SNPs within the 5′ UTR, we identified several SNPs within the coding region causing missense substitutions. We studied these SNPs to investigate if they can provide some insights about their effects on protein structure and thus function. *Zm00001d006065* encodes a basic Helix–Loop–Helix (bHLH) transcription factor 121 (Fig. 2*A*). Protein domain structure analysis using SWISS–MODEL predicted the first helix structure to be from amino acids 158 to 188 curving to the loop structure from amino acids 189 to 197 and then the second helix structure from amino acids 198 to 236 (Fig. 2*C*). A DNA-binding domain is predicted to be between amino acids 167 and 198, while residues between 179 and 236 are predicted to be involved in *ZmbHLH121* homodimerization. However, the missense amino acid substitutions (H330P, F320L, D319E, F275Y, and A256V) lie in the disordered region, downstream of the bHLH domain of the full-length protein. These mutations were also predicted to have low sequence conservation, high mutation tolerance (i.e., they can be readily substituted by other amino acids) and lie away from the predicted pocket (active site) of bHLH (Phyre2 Investigator results) (*SI Appendix,* Fig. S1). Overall, the modeling results suggested that these missense amino acid substitutions are unlikely to have any effect on the function of the protein. This is also corroborated by the phenotypic data of lines showing allelic variations for these SNPs (*SI Appendix,* Figs. S2 and S3).

ZmbHLH121 Is a Positive Regulator of RCA Formation in Maize.
Root expression analysis using a maize expression atlas (40) showed that this gene is highly expressed in the root cortex (Fig. 1 and *SI Appendix,* Fig. S4), suggesting its relevance for the RCA phenotype. To functionally validate the importance of *ZmbHLH121* during RCA formation, we first identified a transposon-tagged mutant line harboring a Uniform Mu transposon insertion in the exon 6 of the *ZmbHLH121* (*ZmbHLH121*-Mu) gene in the maize genotype W22 (Fig. 2*A*). A mutant homozygous for the mu1021839 insertion was obtained and the position of the insertion was verified to be 1,305-bp downstream of the transcriptional start site (*SI Appendix,* Fig. S5). The translated Mu insertion position is downstream of the motifs predicted to be essential for *ZmbHLH121* DNA binding and protein–protein interaction (Fig. 2*C*). Nevertheless, quantification of RCA in roots of field-grown plants of *ZmbHLH121*-Mu found it to have significantly reduced RCA formation compared with its wild-type W22 background (Fig. 3 and *SI Appendix,* Fig. S6).

To confirm that the mutation within *ZmBHLH121* is responsible for the observed phenotypes in the mu transposon line, we generated additional mutants in the maize genotype FBLL MAB genetic background using a CRISPR/Cas9 editing approach (hereafter referred as *ZmbHLH121*-CRISPR). Seven independent transgenic plants were generated carrying the CRISPR/Cas9 transgene. One *ZmbHLH121*-CRISPR mutant was identified with a 5-bp Cas9-induced deletion at the second gRNA target site in exon 3 (Fig. 2*A* and *SI Appendix,* Fig. S7*A*). No significant difference in *bHLH121* transcript levels was observed in the mutant compared with its wild-type background (*SI Appendix,* Fig. S8). However, 5-bp deletion caused a frameshift, leading to formation of a premature stop codon (Fig. 2*B* and *SI Appendix,* Fig. S7*B*). The translated amino acid sequence of the mutant allele thus diverged from the wild-type sequence after amino acid 177; therefore lacking a portion of the predicted DNA-binding motif and all of the protein–protein interaction motif (Fig. 2*C*). The RCA phenotype in roots of the homozygous *ZmbHLH121*-CRISPR mutant was significantly reduced compared with the wild-type FBLL MAB background in the greenhouse (Fig. 4).
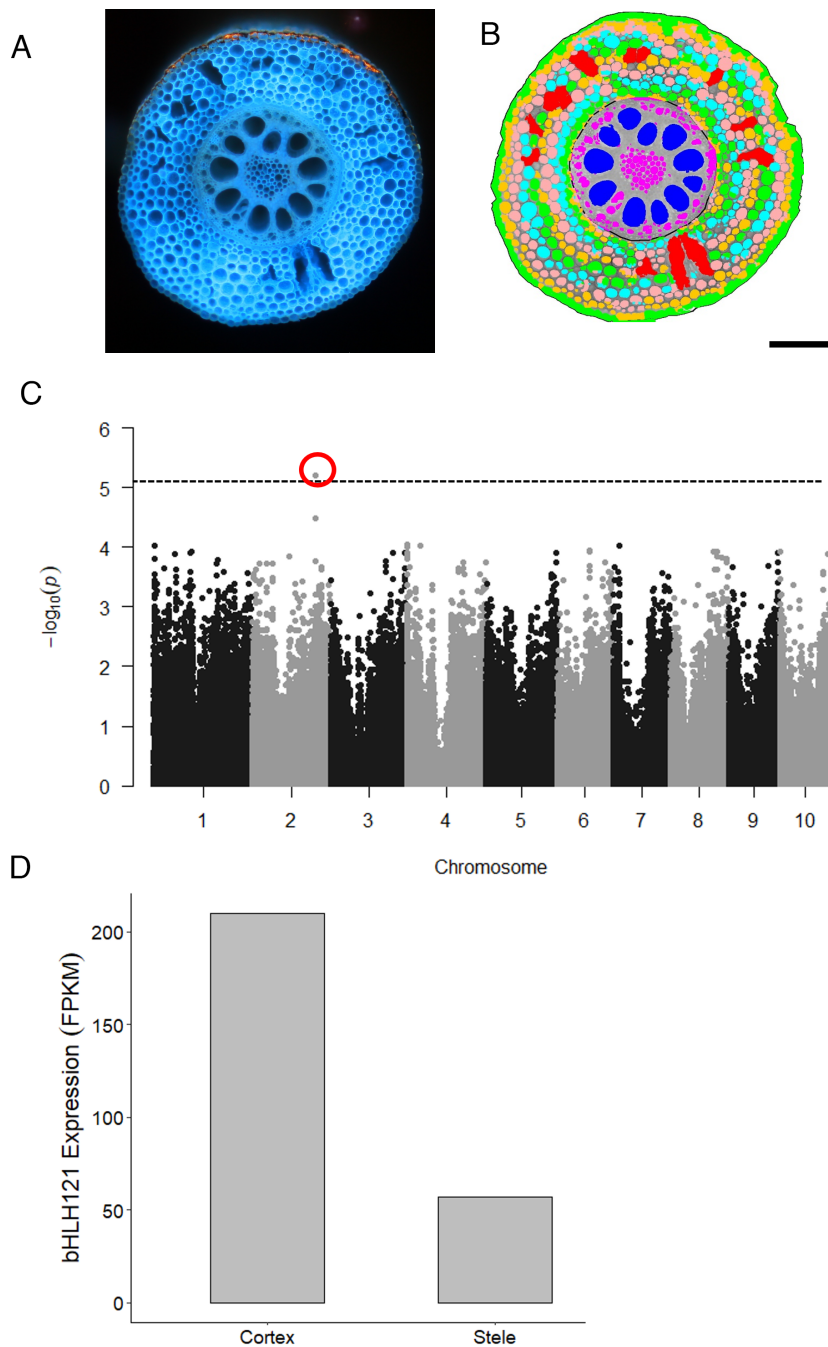
Fig. 1. Identification of mutant locus associated with root cortical aerenchyma in maize roots. (*A*) An image of root cross-sectional surface captured by laser ablation tomography (LAT). (*B*) Root anatomical phenotypes were quantified by *RootScan* software. (*C*) Manhattan plot of GWAS results for root cortical aerenchyma. Chromosome-wide significance threshold (horizontal line) was set using the simple*M* method ($-\log_{10}p$ = 5.32). Significant SNPs were located in gene model GRMZM2G083504 (*ZmbHLH121*) encoding a ZmbHLH121 transcription factor. (*D*) Relative expression of *ZmbHLH121* in the stele and cortex of a primary root from a 3-d-old maize seedling (40). (Scale bar, 100 μm.).

Our mu-transposon and CRISPR mutants suggested that *bHLH121* could play a positive role in regulating RCA formation. To validate this, we generated a transgenic line overexpressing *ZmbHLH121* in the B73 genetic background (referred as *ZmbHLH121*-OX). A homozygous line showed >100 fold increase in mRNA levels of *ZmbHLH121* compared to its wild-type B73 (*SI Appendix*, Fig. S8). Characterization of root anatomy of *ZmbHLH121*-OX grown in the greenhouse under control conditions showed a significant 1.4-fold increase in RCA formation compared with the B73 wild-type (Fig. 2). Overall, these functional validations indicate that *ZmbHLH121* is a positive regulator of RCA formation under controlled conditions in maize.

ZmbHLH121 Controls RCA Formation under Nitrogen and Water-Stressed Conditions. To investigate whether *ZmbHLH121* also regulates RCA formation under environmental stress conditions, we first performed greenhouse experiments under nitrogen and water stress and control treatments with *ZmbHLH121*-OX and *ZmbHLH121*-CRISPR lines and their respective wild types. *ZmbHLH121*-OX had increased RCA formation compared with B73 in all treatments. Both treatments induced RCA formation in both *ZmbHLH121*-OX and its wild-type B73. Interestingly, the bHLH121 overexpression line had 42% RCA formation compared with 30% RCA formation in B73 in control treatments. In low nitrogen and water deficit treatments, *ZmbHLH121*-OX had
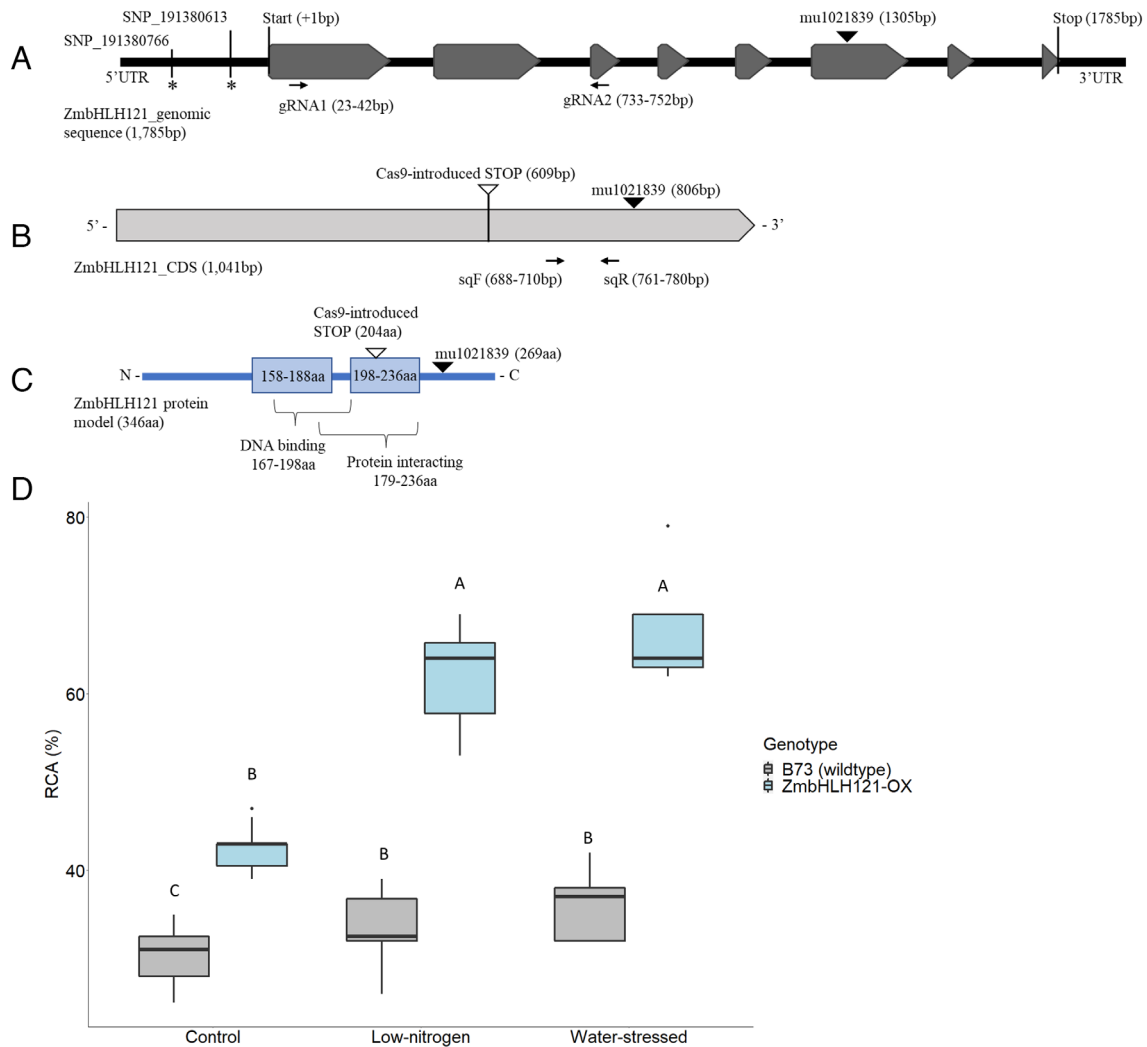
Fig. 2. Predicted gene and protein models of ZmbHLH121. (*A*) Gene model of B73v4 primary bHLH121 primary transcript Zm00001d006065_T001. bHLH121 is 1,785 bp from the start codon to stop codon. It consists of eight exons depicted as gray boxed arrows. Introns and UTRs are depicted as black lines. SNPs identified significantly associated with RCA formation are indicated by the asterisk (*) in the 5′UTR. The black triangle marks the insertion position of the Mu transposon in exon 6. The black arrows below exon 1 and exon 3 mark where guide RNAs (gRNA) target bHLH121 genomic sequence for gene editing. (*B*) bHLh121 coding sequence is 1,041 bp long. The white triangle marks the introduction of a stop codon resultant of CRISPR/Cas9-induced mutation. The black triangle shows the Mu transposon insertion position in the coding sequence. (*C*) Diagram of predicted bHLH121 protein motifs based on homology modeling. bHLH121 is 346 amino acid (aa) long. The blue boxes are the predicted alpha helices and the residues comprising the helices. The predicted DNA binding aa residues are between 158 and 188 while aa residues between 179 and 236 are involved in bHLH121 homodimerization. The white triangle marks the translated position of the stop codon generated from CRISPR/Cas9-induced mutation that results in the production of a truncated bHLH121 protein. The black triangle marks the translated position the Mu transposition insertion site. (*D*) ZmbHLH121-OX had increased RCA formation compared with the wild type (B73) in low-nitrogen, water stress, and control conditions in greenhouse experiments at node 3. Means with the same letters are not significantly different ($P ≤ 0.05$) within the same treatment group according to Tukey's HSD. RCA are presented as percent of cortical area in roots grown in greenhouse experiments.

62% and 67% RCA formation when compared with 22% and 36% RCA formation in B73, respectively (Fig. 2). As anticipated, *ZmbHLH121*-CRISPR grown in controlled conditions had significantly reduced RCA formation when compared with wild-type plants. The *ZmbHLH121*-CRISPR line had 14% RCA formation compared with 46% RCA formation in the FBLL MAB wild-type (Fig. 4). In low-nitrogen conditions, the *ZmbHLH121*-CRISPR mutant had 43% RCA formation compared with 12% RCA formation in wild-type counterparts (Fig. 4). In water deficit conditions, *ZmbHLH121*-CRISPR had 20% RCA formation compared with 48% RCA formation in the wild-type (Fig. 4). We conclude from our loss of function and over expression studies that the bHLH121 protein could function as a positive regulator of RCA formation even under studied environmental stress conditions. RCA formation in these two lines is altered only in node 3 roots (but not in nodes 2 and 4), consistent with the phenotypic data used in the GWAS model.

To confirm that *ZmbHLH121* regulates RCA formation under environmental stress in field conditions, we phenotyped *ZmbHLH121* mutant lines under 6 different environmental conditions (high and low nitrogen, well-watered and water-stressed environments, and two nonstressed environments) in four different field sites (Rock Springs, Arlington, West Madison, and Hancock). *ZmbHLH121*-Mu showed significant reduction in RCA formation under control as well as nitrogen stress compared with the W22 in the Rock Springs and Hancock field sites (Fig. 3). Similarly, differences in RCA formation between *ZmbHLH121*-Mu and W22 were observed in many other field sites and stress conditions (*SI Appendix*, Fig. S6 and Tables S1 and S2). Homozygous *ZmbHLH121*-Mu mutants had less RCA in root node 3 compared with W22 plants in many of these environments, whereas no significant differences were observed for root node 2 or 4 in these environments (*SI Appendix*, Tables S1–S3). This suggests that
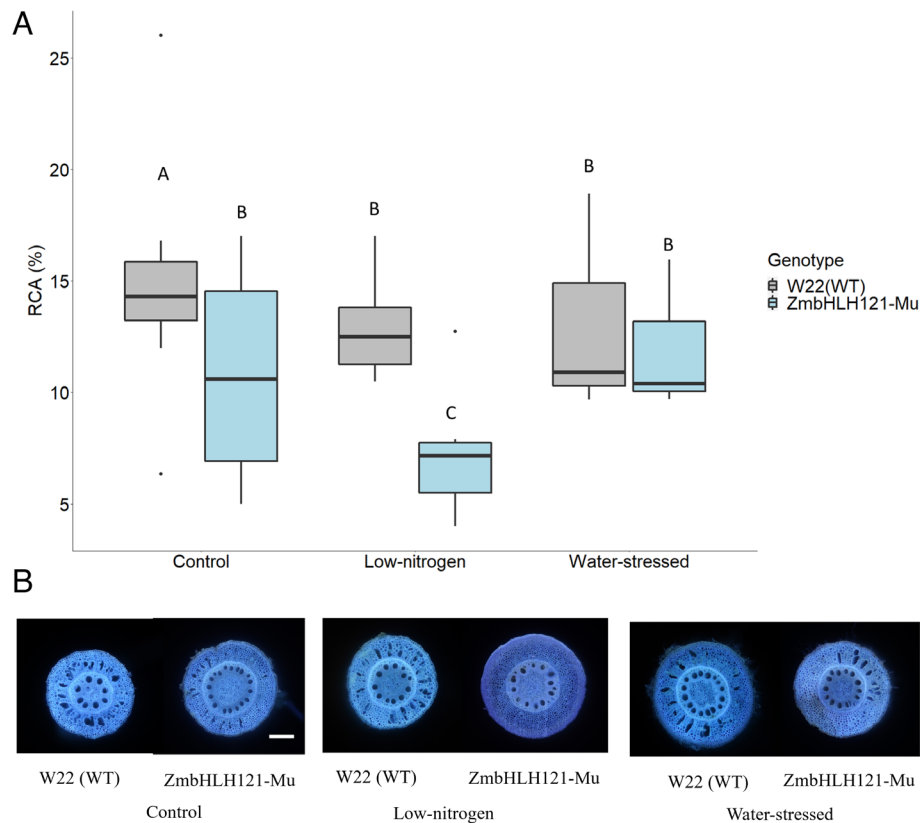
Fig. 3. The bHLH121-Mu had reduced RCA compared with the wild type in the field. (*A*) bHLH121-Mu had reduced RCA formation compared with W22 wild type at third node root in control and low-nitrogen environments. Means with the same letters are not significantly different ($P ≤ 0.05$) within the same treatment group according to Tukey's HSD. (*B*) Representative root cross-section images and quantification of RCA (as percent of cortical area). Root segments were collected 6 to 8 cm from the base of the third whorl crown roots at anthesis. Image of wild-type W22 (WT) and mutant ZmbHLH121-Mu.

ZmbHLH121 could be involved in node-specific regulation of RCA formation.

Discussion

We employed *Anatomics* in combination with GWAS to identify a gene, annotated as *ZmbHLH121,* regulating RCA formation in maize (Fig. 2). This gene encodes a bHLH transcription factor. Temporal and spatial expression analysis of the maize gene expression atlas (40, 41) revealed that the *ZmbHLH121* gene is expressed in roots and shoots. However, *ZmbHLH121* transcript abundance was higher in cortical parenchyma of primary roots, suggesting it may regulate RCA formation. *ZmbHLH121* expression was also up-regulated in the primary root differentiation zone compared with the root apical meristem and elongation zones (*SI Appendix,* Fig. S4), in agreement with the spatial location of RCA formation (40).

Functional evidence for *ZmbHLH121* acting as a regulator of RCA was provided by phenotyping knock-out and overexpression lines (Figs. 2–4 and *SI Appendix,* Fig. S9). *ZmbHLH121*-Mu and *ZmbHLH121*-CRISPR mutants displayed reduced RCA formation while an *ZmbHLH121*-OX mutant displayed enhanced RCA formation in node 3 roots compared with the wild type. Our study suggests that roots originating from different nodes may be under distinct genetic regulation. Overall, these results indicate that the *ZmbHLH121* gene functions as a positive regulator of RCA formation at node 3 in maize roots.

Notably, *ZmbHLH121* controls RCA formation not only in optimal (control) conditions, but also in edaphic stresses. We observed greater contrasts in RCA formation in *ZmbHLH121*-OX mutants when compared with wild-type plants in greenhouse conditions. In contrast, the field-grown *ZmbHLH121*-Mu mutant did not display a consistent RCA phenotype across all environments (*SI Appendix,* Fig. S6). RCA is a highly plastic anatomical phenotype. An array of edaphic stress factors, including hypoxia and suboptimal availability of water, phosphorus, nitrogen, and sulfur, all promote RCA formation (24–28, 42, 43). Differences between growth environments, the timing and severity of edaphic stress, and heterogenous soil nutrient and water distribution in the field may contribute to the large variation in RCA observed within a single genotype (44). This inconsistent phenotype may also be due to the *ZmbHLH121*-Mu insertion line's truncated protein retaining a partial function, a functional redundancy within the bHLH family, or an environmental specificity of gene expression. The mu1021839 insertion is located after the predicted motifs involved in protein–protein interaction and DNA binding (Fig. 2). Thus, production of a truncated *ZmbHLH121*-Mu protein may not inhibit homodimerization.

bHLH proteins belong to a superfamily of transcription factors that are involved in diverse processes including PCD (45). For example, the rice bHLH transcription factor Eternal Tapetum 1 (EAT1) is involved in late pollen development. EAT1 positively regulates PCD in tapetal cells by promoting aspartic proteases triggering plant PCD. Loss of function of EAT1 results in delayed tapetal PCD and aborted pollen development leading to complete male sterility (45). *ZmbHLH121* is orthologous to *Arabidopsis* CRYPOTCHROME 2-interacting bHLH3 (*CIB3*). bHLH TFs such as CIBs are known to bind cryptochromes in light-dependent manner and are linked with cryptochrome signaling. Recent studies have identified that cryptochrome activation by blue light
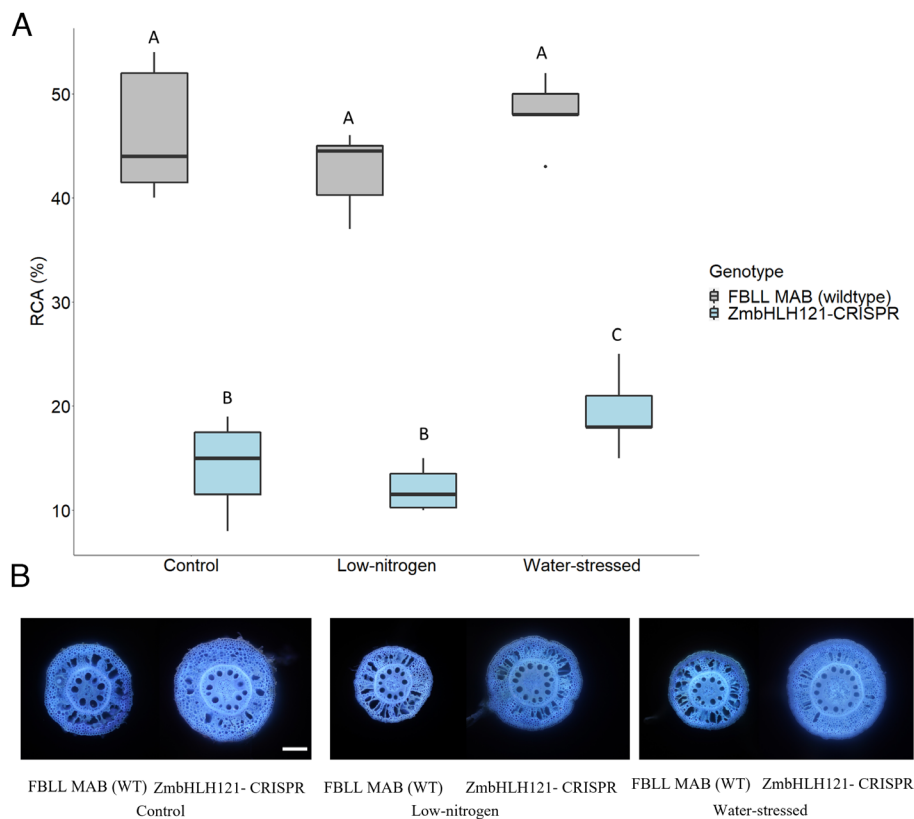
Fig. 4. ZmbHLH121-CRISPR had reduced RCA formation in greenhouse experiments. (*A*) ZmbHLH121-CRISPR had reduced RCA (as percent of cortical area) formation compared with the FBLL MAB wild type in low nitrogen, water stress, and control conditions in greenhouse experiments at node three. Means with the same letters are not significantly different ($P \leq 0.05$) within the same treatment group according to Tukey's HSD. (*B*) Representative root cross-section images. Root segments were collected 6 to 8 cm from the base of the third node crown roots at anthesis. Image of wild-type FBLL MAB (WT) and the CRISPR/Cas9 mutant ZmbHLH121-CRISPR. (Scale bar, 100 μm.).

catalyzes the enzymatic accumulation of reactive oxygen species (ROS) and H_2O_2 serving as a light-activated generator of ROS (46, 47). This cross-species functional data suggest that *ZmbBHLH121* could be involved in an ROS-induced PCD pathway of RCA formation. In maize roots, PCD is a key process leading to RCA formation (24, 48). Our findings suggest that *ZmbHLH121* may promote RCA formation through the PCD pathway. Further studies would be needed to confirm this and determine exactly where in the PCD pathway *ZmbHLH121* may function. RCA formation is well known for facilitating gas exchange in hypoxic conditions (49). However, the formation of RCA also has important consequences for root metabolic costs, and therefore soil resource acquisition (24–29). RCA reduces the metabolic cost of maintaining root tissue, and therefore permits deeper rooting and the capture of mobile resources in deep soil strata, including nitrogen and water (25, 27, 28, 30). In agricultural systems, where water and nitrogen limit plant growth, root phenotypes that enhance root depth improve the capture of mobile resources (50–52). RCA formation may be particularly beneficial for subsoil foraging, as a reduced metabolic cost of root tissue enables exploration in deep soil domains with greater tolerance to hypoxia and tolerance of Mn toxicity by diminishing oxygen depletion in the rhizosphere (and therefore maintaining Mn in a more oxidized state) (13). However, root phenotypes that decrease the metabolic cost of soil exploration are also beneficial for the capture of immobile soil nutrients including phosphorus and potassium (15, 26, 29).

The utility of RCA formation for the capture of specific nutrients is dependent on the interaction with architectural phenotypes that localize root foraging in specific soil domains (14). A recent study showed that multiple integrated root phenotypes, including phenotypes with high RCA formation, cooptimize drought tolerance in maize (53). In maize, lateral root branching and RCA interact to improve plant performance under suboptimal nitrogen availability (26). The number of nodal roots and RCA interact synergistically to increase plant growth greater than the expected additive effects (7). Identifying the genetic control and functional significance of genes controlling RCA formation will aid in developing crop varieties with improved edaphic stress tolerance.

The expression of root anatomical phenotypes varies by node (54). Our study suggests that roots originating from different nodes may be under distinct genetic control, as RCA phenotypes were observed in node 3 and not nodes 2 and 4 (*SI Appendix*, Tables S1–S3). The expression of different phenotypes on different nodes may also depend on ontogeny. It has been suggested that node-specific expression of phenotypes and stress responses could reflect developmental transitions, which require further study (54, 55). Phenotyping root phenotypes on individual nodes are essential for understanding the functional utility and genetic control of root phenotypes.

Earlier studies employing quantitative genetic analysis for constitutive aerenchyma formation have identified Quantitative Trait Loci (QTL) on chromosome 1, 5, and 8 in maize × *Zea nicaraguensis* mapping populations (32). An additional QTL for aerenchyma area was identified on chromosome 8 in a maize recombinant inbred population (33). However, to date, only a flooding-induced gene encoding a xyloglucan endo-trans-glycosylase (*xet1*) has been associated with RCA formation in maize (56). Evidence from biochemical studies and microarray analyses indicates that several genes related to the generation or scavenging of reactive oxygen species,

cell signaling, cell wall modification, ethylene pathway, and proteolysis are differentially expressed during aerenchyma formation (57, 58). *ZmbHLH121* may function upstream to regulate these processes.

RCA formation is a common phenomenon in maize, rice, wheat, sorghum, and many other *Poaceae* (27, 59–61). Therefore, we expect these results to help inform the genetic control of RCA in several other species. The phylogenetic analysis revealed close *ZmbHLH121* orthologs in millets, sorghum, sugarcane, and silver grass (*SI Appendix*, Fig. S10). These species have been shown to form RCA (62–65). In addition, Zm00001d021019 is the closest paralog of Zm00001d00060065 (*ZmbHLH121*) in maize with >75% protein identity. The longer branch length of *ZmbHLH121* compared with Zm00001d021019 suggests that *ZmbHLH121* has diverged further from Zm00001d021019 (*SI Appendix*, Fig. S10). The expression analysis suggests that *ZmbHLH121* is maximally expressed in the root while Zm00001d021019 is maximally expressed in germinating kernels (66). However, their expression in different root zones and tissues shows overlapping patterns, with Zm00001d021019 showing lower expression compared to *ZmbHLH121*. This may suggest that there could be a functional redundancy between Zm00001d021019 and *ZmbHLH121*, which may explain why complete RCA suppression was not observed in the *ZmbHLH121*-CRISPR mutant. Other genes likely play a role in aerenchyma formation and other PCD processes, quantitative traits that are tightly regulated by growing plants.

In summary, despite their potential as target traits for plant breeding, little is known about the genes that regulate root anatomical phenotypes in crops. This is primarily because of the practical difficulties in obtaining thousands of root samples, imaging cross-sections, and quantifying root phenotypes. Here, we demonstrate how a combination of *Anatomics* and GWAS of field-grown plants led to the identification of *ZmbHLH121*, a regulatory gene controlling RCA formation. bHLH family members have previously been shown to be involved in PCD, which is an important developmental process in aerenchyma formation (24, 45). We validated our GWAS results by characterizing RCA formation in *ZmbHLH121* loss-of-function and overexpression mutants. These observations indicated that *ZmbHLH121* functions as a positive regulator of RCA formation, consistent with our expression analysis where its transcript was more abundant in older root cortical tissues where RCA forms. Understanding the genetic control of root anatomical phenotypes may enable the development of more productive crop cultivars that are resilient to edaphic stress.

Materials and Methods

Plant Materials and Growth Conditions. Four hundred and thirty-six maize lines of the Wisconsin Diversity Panel were employed in this study (67) (*SI Appendix*, Table S4). Experiments were conducted from January to April of 2011 and 2012 and from November to February of 2013 at the Ukulima Root Biology Center (URBC) in Alma, Limpopo province, ZA (24°33′ 00.12 S, 28° 07′25.84 E, 1235 masl) using a randomized complete block design with two replications in each year. The soil at the experimental site is a Clovelly loamy sand (Typic Ustipsamment). Each maize line was planted in a single-row plot consisting of 20 plants per plot. Row width was 75 cm, and distance within a row was 23 cm. In all trials, soil nutrient levels were adjusted to meet the requirements for maize production as determined by soil tests at the beginning of the growing seasons. The trials were irrigated using a center pivot system. Pest and disease control was implemented as needed.

Root Sampling. Roots were sampled 7 to 8 wk after planting. Root excavation was carried out using "shovelomics" (35). Three representative plants were selected for excavation in each plot. The selection was based on height, presence of bordering plants, and general appearance that represented individuals in the plot.

Root crowns were collected by carefully removing a soil monolith containing the intact roots. The monolith was 30 cm in diameter by 15 cm deep centered on the stem. A large portion of the soil was removed from the roots by careful shaking. The remaining soil was removed by soaking the roots in diluted commercial detergent followed by vigorously rinsing at low pressure with water. A 4-cm root segment was collected 8 cm from the base of the second or third node crown roots. The samples were stored in 70% (v/v) ethanol in water at 4 °C until processing and analysis.

Laser Ablation Tomography and Image Capture. Laser ablation tomography (LAT) was used to obtain cross-sectional images of all root samples (36, 37). This LAT platform combined a nanosecond pulsed UV laser (Avia 355-7000; Coherent) focused into a beam using a galvanometer scanner (HurryScan 10; Scanlab) for surface ablation of the sample, a three-axis motorized stage (ATS100-100; Aerotech Inc.) to position and move the sample, and a camera (Canon EOS Rebel T3i; Canon USA Inc.) and macro lens (65 mm MP-E 1-5X variable magnification; Canon USA Inc.) for image capture. The scale for all images at this magnification was 1,173 pixels per mm. Each root segment was secured on the stage perpendicular to the laser beam using a notched microscope slide, moved into the beam at 30 μm s^{-1} for 10 s while images were captured, and three cross-sectional images per root were saved for analysis.

Quantification of Root Anatomical Phenotypes. Root anatomical phenotypes were quantified using the semiautomated image analysis program *RootScan* (38) for GWAS experiments and *RootScan2* (https://plantscience.psu.edu/research/labs/roots/methods/computer/rootscan) for mutant studies. The analysis of images was performed in MatLab 7.6 2008a (The MathWorks Company). *RootScan* and *RootScan2* separate different types of root tissues using pixel thresholds. Cortical area and aerenchyma area were calculated via pixel counting. Pixel values were converted to mm or mm^2, based on micrometer calibration (1,173 pixels/linear mm). Primary measurements were used to calculate secondary measurements in *RootScan* and *RootScan2*: percent root cortical aerenchyma (RCA) (total aerenchyma area/total cortical area). No significant differences were observed in plant performance and anatomical phenotypes of *ZmbHLH121*-CRISPR, *ZmbHLH121*-OX, and *ZmbHLH121*-Mu when compared with the wild type (*SI Appendix*, Table S5).

Statistical Analysis. Statistical analyses were performed using R software (version 2.15.1) (68). Root phenotypes were averaged on the plot level. Tukey's HSD test was used for multiple comparison barplots and was conducted using the package *agricolae* (69). A cross-year ANOVA of RCA was applied to analyze genotype, treatment, year, and environment for transposon mutant experiments using *lmerTest* (70). Treatment and genotypes were considered to be fixed effects and replicates and year were random effects. Broad-sense heritability (H^2) on an entry mean basis was calculated according to ref. 71.

$$H^2 = \frac{\sigma^2(G)}{\frac{\sigma^2(E)}{ry} + \frac{\sigma^2(GY)}{r} + \sigma^2(G)},$$

where $\sigma^2(G)$ is the genotypic variance, $\sigma^2(GY)$ is the genotype by year variance, $\sigma^2(E)$ is the error variance, r is the number of replicates per year, and y is the number of years.

Best linear unbiased predictors were calculated for each treatment and environment using a random-effects linear model in the R package *lme4* (72) and used for GWAS analysis.

$$y_{ijk} = \mu + c_i + g_j + bk(i) + (c \times g)_{ij} + e,$$

where y_{ijk} is the predicted response, μ is the grand mean, c is the effect of year, g is the effect of genotype, b is the effect of replication.

Genome-Wide Association Analysis. A GWAS was performed with 436 lines of the Wisconsin Diversity Panel using a set of 438,222 RNA-seq based SNPs (67, 73). Prior to the GWAS, data were power-transformed using the lambda identified by Box-cox transformations. GWAS was performed with the Genomic

Association and Prediction Integrated Tool (GAPIT) package in R using a mixed linear model written as follows (74)

$$y = X\beta + Wm + Qv + Zu + e,$$

where y is a vector of phenotypic observations; β is a vector of unknown fixed effects other than the SNP under testing, m is a vector of fixed marker effect (e.g., SNP), v is a vector of subpopulation effects, u is a vector of unknown random effects, e is a vector of residual effects. Q is an incidence matrix of principal component scores (eigenvectors) of marker-allele frequencies. X, W, and Z are incidence matrices of ones and zeros relating y to β, m, and u, respectively. The covariance of u is equal to KVA, where K is the kinship matrix that was estimated with a random set of SNPs according to the VanRaden method and VA is the additive variance estimated with restricted maximum likelihood. The kinship matrix estimation and the principal component (PC) analysis were performed with the GAPIT package. The optimum number of PCs/covariates to include for each phenotype was determined by forward model selection using the Bayesian information criterion. Allelic effects are estimated relative to the minor allele and a minimum minor allele frequency of 0.05 was used. We implemented the simpleM method (75), which applies a Bonferroni correction to the effective number of independent tests, to determine the genome-wide significance threshold.

Expression patterns of gene models associated with the significant SNPs and their adjacent genes were examined using a comprehensive atlas of global transcription profiles across developmental stages and plant organs database (40, 41). Genes were annotated using R Software (version 3.2.4) (R Core Team 2018), Bioconductor (76), MapMan (77), and MaizeGDB (78). Candidate genes identified through significant GWAS hits were detected based on the physical position of genes in the version 4 B73 (AGPv4) reference sequence assembly (79).

***ZmbHLH121* Secondary Structure and Phylogenetic Analysis.** MaizeGDB was used to identify the predicted primary transcript of *ZmbHLH121* (GRMZM2G083504_T002 associated with AGPv3, Zm00001d006065_T001 associated with AGPv4). The translated amino acid sequence of Zm00001d006065_T001 (UniProt database, https://www.uniprot.org, ID Q9LT23) was used for analysis of secondary structure on Phyre2 (http://www.sbg.bio.ic.ac.uk/phyre2), SWISS-MODEL (https://swissmodel.expasy.org/), and NCBI PSY-BLAST (https://blast.ncbi.nlm.nih.gov) using standard parameters on respective servers. All secondary structure outputs were similar and thus we present the secondary structure analysis from SWISS-MODEL. Most of the protein, except the bHLH domain between residues 158 and 236, was predicted to be disordered and was thus approximated to a random coil confirmation. Further, the bHLH121 protein sequence was submitted to HPEPDOCK (http://huanglab.phys.hust.edu.cn/hpepdock/), a protein–protein docking server. The missense amino acid substitutions indicate no formation of the protein–protein interaction interface.

SWISS-MODEL used 6GII.pdb (Microphthalmia-associated transcription factor) as the top template for the modeling (sequence coverage and identity at 21% and 30.5%, respectively) and predicted a homo-dimer structure for the bHLH domain with a QSQE score of 0.29. The QSQE score is a number between 0 and 1 and reflects the expected accuracy of the interchain contacts for a model; higher numbers indicate higher reliability. Phyre2 used 5GNJ.pdb (transcription factor myc2) as the top template for the modeling (sequence coverage and identity at 21% and 33% respectively) and predicted the bHLH domain structures with a 99.6 confidence score (*SI Appendix*, Fig. S11).

Phylogenetic analysis of bHLH121 orthologous protein sequences in selected cereals and wider species was performed. *ZmbHLH121* was used as a seed gene to select orthologous genes (*E value* < 1E-50 and *Bit-score* > 200) from several monocot species and wider using the interactive phylogenetic module of Monocots Plaza 4.5 (80). Protein sequences were aligned using MUSCLE (81) and a tree was constructed using the FastTree (82) algorithm. The generated Newick file was imported into iTOL (83) to create a rectangular tree.

Development of the *ZmbHLH121*-Mu Transposon Mutant Line and Identification of Mu Insertion Position. The Mu transposon *zmbhlh121* (*ZmbHLH121*-Mu) mutant allele was identified in Uniform-Mu stock mu1021839::Mu (stock ID: UFMu-01678), which was obtained from the Maize Genetics Stock Center-Uniform Mu collection (84). Seeds from the Stock Center were grown at West Madison Agricultural Research Station,

Madison, WI, USA (Latitude: 43°03'37″N; Longitude: 89°31'54″W) during the summer of 2014 and genotyped for the target transposon insertion. Fifty milligram of leaf tissue from each plant was harvested, flash frozen in liquid nitrogen, and ground to a fine powder for DNA extraction in a 1.6-mL microcentrifuge tube using a sterilized 7-cm polypropylene pellet pestle (Grainger). DNA was isolated by the CTAB method, and all primers were designed using Primer 3 based on the B73 AGPv3reference sequence. Plants carrying the mutant allele were identified by genotyping with an outward-facing primer recognizing the terminal inverted repeat (TIR) of the Mutator transposon, TIR6 (5′-AGAGAAGCCAACGCCAWCGCCTCYATTTCGTC-3′) and the *ZmbHLH121* gene-specific primer *ZmbHLH121*_R3 (5′-TTTCAGCTCGCAGTCGCAGTCGCAGG-3′). The wild-type allele was identified using the gene-specific primer set *ZmbHLH121*_F2 (5′-TCCAGTCGCTGCAGCAGCAAGTTGAGG-3′) and *ZmbHLH121* R3. PCR conditions were 95 °C for 30 s, 63 °C for 30s, 72 °C for 45 s, repeated for 30 cycles. The progeny of plants that tested homozygous positive for the insertion were used for phenotype analysis.

The insertion position of the Mu transposon was verified in a homozygous *ZmbHLH121*-Mu family. Fifty milligram of leaf tissue was harvested, frozen, and ground (see above). DNA was extracted using the IBI Genomic DNA Mini Kit according to the manufacturer's instructions. Regions flanking the Mu transposon insertion site were PCR amplified using Phusion™ High-Fidelity DNA polymerase (Thermo Fisher Scientific) according to the manufacturer's recommendations. The region upstream of the Mu transposon insertion site was amplified using the forward primer *ZmbHLH121*-Mu_F (5′-CATAAACTACGTCCAGTCGC-3′) with the TIR6 primer. The region downstream of the Mu transposon insertion site was amplified with the reverse primer *ZmbHLH121*-Mu_R (5′-GTACTAAAAGCCCATCCTCCTC-3′) with the TIR6 primer. PCR conditions were 95 °C for 30 s, 60 °C for 30 s, 72 °C for 2 min, and repeated for a total of 35 cycles. PCR amplicons were column cleaned using the Gel/PCR DNA Fragment Extraction Kit (IBI Scientific) according to the manufacturer's instructions. "A" overhangs were added to the PCR amplicons using 2X Platinum II Taq Hot-Start PCR Master Mix (Thermo Fisher Scientific), TA cloned into pCR2.1 (Thermo Fisher Scientific), and transformed into *Escherichia coli* DH5α. Plasmids were isolated using the Hi-Speed Plasmid Mini Kit (IBI Scientific) and sent to Massachusetts General Hospital DNA Core facility for sequencing.

Construction of *ZmbHLH121*-Overexpression and *ZmbHLH121*-CRISPR/Cas9 Plasmids. The transgene construct used to overexpress *ZmbHLH121* (*ZmbHLH121*-OX) was generated based on GRMZM2G083504_T002 transcript with 128 bp of the 5′UTR fused upstream of the start sequence (*SI Appendix*, Fig. S12A). A Gateway® compatible full-length CDS sequence was synthesized by GeneArt® (Thermo Fisher Scientific). A Gateway® L-R (Thermo Fisher Scientific) reaction was conducted to move the synthetic sequence from the Entry vector pDONR™ ZEO_*ZmbHLH121*-OX to the Destination vector pANIC6D (85) to generate the final plasmid construct pANIC6D_*ZmbHLH121*-OX according to the manufacturer's instructions (*SI Appendix*, Fig. S13A). In this vector, *ZmbHLH121* expression is regulated by the maize *Ubiquitin1* (*ZmUbi1*) promoter with intron 1 enhancer (pACH25) (86), and terminated by the *Octopine Synthase* (*OCS*) termination (pEarlyGate 304) (87), sequence from *Agrobacterium tumefaciens*. The *Phosphinothricin acetyltransferase* (*PPT*) gene (pMDC123) (88) encodes for Bialaphos herbicide resistance. Its expression is regulated by the rice *Actin1* (*OsAct1*) promoter with intron 1 enhancer (pCOR113) (89) and terminated by the *Cauliflower Mosaic Virus 35S* (*CaMV35S*) termination (pMDC123) (88) sequence. The *Red Fluorescent Protein* (*pporRFP*) gene (90) from *Porites porites* is the visual marker. Its expression is regulated by *Panicum virgatum Ubiquitin1* (*PvUbi1*) promoter with intron 1 enhancer (91) and terminated by the *Nopaline Synthase* (*NOS*) terminator (pCAMBIA 1305.2, Cambia) from *Agrobacterium tumefaciens*.

The CRISPR/Cas9 pTRANS240B base vector was generated by replacing the hygromcin (*HPT*) plant selection cassette of pTRANS240 (92) with the *PPT* plant selection cassette from pANIC8D. One microgram of pTRANS240 was digested for 18 to 24 h with *Ase*I and *Ale*I to excise the *HPT* selection cassette. The digested plasmid was column cleaned using an IBI Gel/PCR DNA Fragment Extraction Kit according to the manufacturer's instructions. The PPT plant selection cassette was PCR cloned from pANIC8D as two separate DNA fragments using primers listed in *SI Appendix*, Table S6 with Phusion™ High-Fidelity DNA Polymerase (Thermo Fisher Scientific). In brief, 50 μL reaction volumes were set-up containing 50 ng of pANIC8D plasmid template with 5XHF buffer and primer concentrations

according to the manufacturer's instructions. An annealing temperature of 60 °C was used for a total of 35 PCR cycles. The amplified DNA fragments were column cleaned and pieced together with the digested pTRANS240 backbone via Gibson Assembly (NEB) to generate pTRANS240B according to the manufacturer's instructions. Guide RNAs (gRNAs) were designed to target the *GRMZM2G083504* Exon 1 (5′-GGATGAGCCCATGAGCAGGCTGG-3′) anti-sense DNA strand and Exon 3 (5′-GAAGAGAGAAGATTAGCCAGAGG-3′) sense DNA strand. The gRNAs were cloned into pMOD_B2103 according to Čermák et al. (92), generating pMOD_B2103_*ZmbHLH121*-gRNAs. Each gRNA unit is flanked by the *Csy4* endonuclease recognition sequence that produces a polycistronic gRNA sequence. Expression of the multi-gRNA sequence is regulated by the *Cestrum Yellow Leaf Curling Virus* (*CmYLCV*) promoter (93) and terminated by the *CaMV35S* terminator. A final Golden Gate was done according to Čermák et al. (92) assembling pTRANS240B, pMOD_A1510, pMOD_B2103_bHLH121-gRNAs, and pMOD_C3102 to generate the binary plasmid *ZmbHLH121*-CRISPR (*SI Appendix*, Fig. S13C). pMOD_C3102 carries the red-shifted *Green Fluorescent Protein* (*GFP6*) visual marker. Expression of *GFP6* is regulated by *PvUbi1* and terminated by *Pisum sativum RuBisCO small subunit E9* (*pea rbcS*) terminator.

Generation of Transgenic Maize Lines. Transgenic plants carrying the *ZmbHLH121*-OX transgene were generated using maize genotype Hi-II (AxB) via *Agrobacterium tumefaciens*-mediated transformation (94). The primary transgenic maize plants were grown at the University of Wisconsin-Madison Walnut Street Greenhouse, Madison, WI, USA (Latitude: 43°04′35.8″N; Longitude: 89°25′25.3″W) in 11.4 L pots filled with Berger BM2 potting mix at 25 °C under 18:6-h light–dark cycle. Mature transgenic plants were outcrossed with B73 to generate backcross 1 (BC1) seeds. BC1 seeds were sorted based on RFP signal using a Nightsea Dual Fluorescent Protein Flashlight. Seeds that exhibited RFP fluorescence were considered transgenic and were retained. Seeds not exhibiting RFP fluorescence were considered nontransgenic. Transgenic BC1 seeds were field-grown during the summer of 2016 at the West Madison Agriculture Research Station. Plants were cross-pollinated with B73 to generate BC2 seeds. BC2 seeds were sorted based on RFP fluorescence to identify transgenic seeds. Transgenic BC2 seeds were grown in the University of Wisconsin-Madison Wisconsin Crop Innovation Center (WCIC), Middleton, WI, USA (Latitude: 43°05′56.0″N; Longitude: 89°31′59.8″W) greenhouse in the winter of 2017/2018 in 11.4 L pre-filled pots (Carlin Horticultural Supplies, Milwaukee, WI, USA) at 25 cC under 18:6-h light–dark cycle. Transgenic plants were self-pollinated to generate BC2 filial 1 (BC2F1) progenies. BC2F1 seeds were sorted based on RFP signal. Seeds positive for RFP fluorescence are transgenic while sibling seeds with no RFP fluorescence are nontransgenic. BC2F1 transgenic *ZmbHLH121*-OX and nontransgenic seeds were field grown at the West Madison Agriculture Research Station in 2017, 2018, and 2019. Progenies from BC2F1 generation were maintained through single-seed descent to generate transgenic *ZmbHLH121*-OX BC2F4 and nontransgenic *ZmbHLH121*-OX BC2F4 seeds used in this study.

Transgenic plants carrying the *ZmbHLH121*-CRISPR transgene were generated *via Agrobacterium tumefaciens*-mediated transformation using the maize FBLL MAB genotype according to Lowe et al. (95). Primary transgenic plants were grown in WCIC greenhouses and backcrossed with FBLL MAB pollen in winter of 2017/2018 to generate BC1 seeds. BC1 progenies were grown in WCIC greenhouses in spring of 2018 and backcrossed with FBLL MAB pollen. BC1 plants were genotyped for presence of Cas9-induced mutations. BC2 plants verified to have CRISPR/Cas9-induced mutations were grown in WCIC greenhouses in fall 2018, and BC2F1 progenies were generated by self-pollination. Segregating BC2F1 progenies were field grown at West Madison Agriculture Research Station in summer of 2019 and genotyped to identify mutants homozygous for the *ZmbHLH121*-CRISPR mutation. All BC2F1 plants were self-pollinated to generate the BC2F2 generation.

Genotyping for Presence of Cas9-Induced Mutations in the *ZmbHLH121*-CRISPR Line. Leaf tissue was sampled from primary transgenic plants carrying the *ZmbHLH121*-CRISPR transgene into 1.6-mL microcentrifuge tubes, flash frozen in liquid nitrogen, and stored at −80 °C. Fifty milligram of frozen leaf tissue was ground to a fine powder for DNA extraction in a 1.6-mL microcentrifuge tube using a sterilized 7-cm blue polypropylene pellet pestle (Grainger). DNA was extracted using the IBI Genomic DNA Mini Kit for plants according to the manufacturer's instructions. The T7 Endonuclease I (T7EI) assay (96) was used to detect Cas9-induced mutations in the targeted regions of *ZmbHLH121*. Primers designed to flank the

CRISPR/Cas9 gRNA1 target site (Forward: 5′-ACAGCGACTACATTGCCAGC-3′, Reverse: 5′-TTCTGCGCTTTGACTTCAAC-3′) yielded a PCR product of 502 bp and primers flanking CRISPR/Cas9 gRNA2 target site (Forward: 5′-CCAAAGACTACGTCCATGTC-3′, Reverse: 5′-CCACCCGAGCCAAAGCTGTG-3′) yielded a PCR product of 795 bp. Fifty nanogram of total DNA was used in 50 μL PCR using Phusion™ High-Fidelity DNA polymerase (Thermo Fisher Scientific) following conditions suggested by the manufacturer. The annealing temperature was set to 60 °C and the PCR cycled for 35 cycles. PCR products were then column cleaned using the IBI Gel/PCR DNA Fragment Extraction Kit and eluted with 20 μL RNAse-free water. Column-cleaned PCR products were denatured in a gradient thermocycler at 95 °C for 5 min, rapidly cooled to 85 °C at −2 °C s^{-1}, and then slowly cooled to 25 °C at −0.1 °C s^{-1}. Ten microliter of annealed PCR products were digested with T7EI (NEB) for 2 h and separated by 1% agarose gel electrophoresis.

qRT-PCR Analysis of *ZmbHLH121* Expression in CRSIPR Mutant and *ZmbHLH121*-OX Lines. For the over expression line and wild-type (B73), seeds were sown directly into M3 compost and grown for 1 mo in the greenhouse. Two cm from the tip of the emerging leaf was harvested from three plants for each line and flash frozen in liquid nitrogen. For the CRISPR and wild-type (FBLL), seeds were surface sterilized (70% ethanol for 5 min, 15% bleach for 5 min, five water washes) and grown on a damp filter paper for 5 d. One centimeter was excised from the tip of the roots and shoots and flash frozen in liquid nitrogen.

RNA was extracted using the MonarchR Total RNA Miniprep Kit (NEB, T2010S) as per protocol and cDNA generated using the Thermo Scientific Revertair first strand cDNA synthesis kit. Quantitative RT-PCR analysis was performed on a qTOWER 384G machine (Analytikjena) using SYRBgreen (Meridian bioscience, Sensimix SYBR Hi-ROX Kit). Primers for bHLH121 (Zm00001d006065) and two internal control genes Actin 1 (Zm00001d010159) and MEP (Zm00001d018359) were used (*SI Appendix*, Table S7).

Investigation of *ZmbHLH121*-Mu, -OX, and -CRISPR Response Under Different Field and Greenhouse Conditions. *ZmbHLH121*-Mu and W22 wild-type control plants were grown at West Madison Agricultural Research Station during the summer of 2015, Hancock Agricultural Research Station during the summer of 2019, Arlington Agricultural Research Station during the summer of 2018, and Russell E. Larson Agricultural Research Center in Rock Springs, PA, USA during the summers of 2015, 2016, 2017, 2018, and 2019. Field experiments at the West Madison Agricultural Research Station and Arlington Agricultural Research Station (43° 18′ 9″.74 N, 89° 20′ 43″.32 W) (Plano silt loam (fine-silty, mixed mesic Typic Arguidoll) were completed as control conditions. Field experiments at the Hancock Agricultural Research Station [44° 07′ 56″.74 N, 89° 30′ 43″.96 W, 331 masl, plain-field loamy sand (mixed, mesic Typic Udipsamment)] were conducted in low- and high-nitrogen and well-watered and water-stressed environments. Field experiments at the Russell E. Larson Agricultural Research Center (Latitude: 40° 42 ′37″.52 N; Longitude: 77° 57′ 07″.54 W) (Hagerstown silt loam: fine, mixed, semi active, mesic Typic Hapludalf) were conducted in low- and high-nitrogen environments in 2015, 2016, 2017, 2018, and 2019 and in well-watered and water-stressed environments in 2018 and 2019. All field experiments were conducted from May to August. Each genotype was grown in 3-row plots consisting of 60 plants per plot. Genotypes were grown in four replications randomized within each split plot. Row width was 75 cm, and distance between plants within a row was 23 cm. At anthesis, three plants per plot were excavated using the shovelomics method (35). Shoot biomass was collected, dried at 60 °C for 5 d, and weighed. Root samples were collected at 8 cm from the base of the second, third, and fourth node crown roots at anthesis. The samples were stored in 70% (v/v) ethanol in water at 4 °C until processing and analysis. Three images were captured per root and analyzed with *RootScan2*.

For nitrogen field experiments, there were four blocks (0.4 ha area each) split across two fields in Rock Springs, PA. On the low-nitrogen half of each field, no nitrogen fertilizer had been applied since 2010, and this was designated as the low N treatment (10 mg NO$_3^-$ kg^{-1}, as determined through soil tests). The high-nitrogen side of the field had 146 kg ha^{-1} nitrogen applied annually (23 mg NO$_3^-$ kg^{-1}, as determined through soil tests). Field soil was collected at 10 and 30 cm depth, air-dried, homogenized, and samples of equal mass were tested for nitrate content was using a LAQUA Twin nitrate meter (Spectrum Technologies).

For water deficit field experiments at Rock Springs, PA, the rainout shelters (10 × 30 m) covered with a clear polyethylene film were automatically triggered

by rainfall to cover the plots (https://youtu.be/z2McVTsgR4g). These shelters excluded natural precipitation from 3 wk after planting until grain harvest. Adjacent nonsheltered plots were drip-irrigated as needed to provide unstressed comparisons. Soil water status of sheltered and nonsheltered plots were monitored weekly by time domain reflectometry (TDR) probes buried at 15- and 30-cm soil depth. Probes were calibrated to gravimetric soil samples. The well-watered treatments had on average 26% and 27% soil moisture at 15- and 30-cm soil depth, respectively. The water-stressed treatments had on average 16% and 21% soil moisture at 15- and 30-cm soil depth, respectively.

Greenhouse experiments to confirm the phenotype of the mutant, *ZmbHLH121*-OX, -CRISPR and wild-type plants (FBLL MAB and B73) were conducted in a greenhouse at University Park, PA (Latitude: 40° 45' 36.0" N, Longitude: 73° 59' 2.4" W). Plants were grown with a 14-h photoperiod, 28 °C/26 °C day/night temperature, 40% RH, and PPFD of 500 μmol m^{-2}s^{-1} measured at the height of the sixth fully expanded leaf. Wild-type and knockout or overexpression genotypes were planted in a split plot design in two treatments (high and low nitrogen or well-watered and water-stressed). Individual plants were grown in pots (i.e., polyvinyl chloride cylinders with an inner diameter of 15.5 cm and height of 1.54 m lined with a transparent 6-mm high-density polyethylene film to facilitate sampling. Pots were filled with 30 L growth medium consisting of 50% commercial grade medium sand (US Silica, USA), 27% horticultural grade fine vermiculite (D3, Whittemore Companies Inc., Lawrence, MA, USA), 18% field soil, and 5% horticultural grade super coarse perlite (Whittemore Companies Inc.), by volume.

In nitrogen stress greenhouse experiments (June to July 2015 and April to May 2017 for *ZmbHLH121*-Mu, April to May 2020 for *ZmbHLH121*-OX, -CRISPR), plants were fertigated with one of two nutrient solutions using drip rings (nutrient solution is listed in *SI Appendix*, Table S8). Nutrient solutions were adjusted to pH 6.0 using KOH and maintained at this pH with KOH or HCl as needed. Each pot was fertigated with 100 mL per pot daily.

In water deficit greenhouse experiments (March to April 2015 and April to May for *ZmbHLH121*-Mu, April to May 2020 for *ZmbHLH121*-OX, -CRISPR), each pot was watered with approximately 100 mL daily. For the water stress treatment, water was withheld starting 14 d after planting until the end of the experiment. Mineral nutrients were provided by mixing the medium with 70 g per pot of Osmocote Plus fertilizer (5 to 6 mo release, Scotts-Sierra Horticultural Products Company, Marysville, Ohio, USA) consisting of (%): NO$_3$ (8) NH$^+$ 4(7), P (9), K (12), S (2.3), B (0.02) Cu (0.05), Fe (0.68), Mn (0.06), Mo (0.02), and Zn (0.05). For water deficit experiments, samples for

gravimetric soil water content were collected at the end of the experiment. Soil samples in 10-cm increments by depth were collected from the soil surface to the bottom of the container, weighed, dried at 60 °C for 72 h, and weighed again. On average, the water-stressed treatment had 4.2% soil moisture and the well-watered treatment had 16.4% soil moisture.

For both water deficit and nitrogen stress greenhouse experiments, each pot was saturated with 2.5 L of water 1 d prior to planting. Two seeds were directly sown into each pot, and plants were thinned 1 wk after planting. For each experiment, a *ZmbHLH121*-OX, -Mu, and/or -CRISPR line in addition to a wild-type line was planted in four replications. At harvest (i.e., 43 to 45 d after planting), the shoot was removed, the plastic liner was extracted from the pot, cut open, and the roots were washed by rinsing the medium away with low-pressure water. Anatomical samples were collected from individual nodes (1 to 4) at 6 to 8 cm from the root base and stored in 70% (v/v) ethanol at 4 °C until processing and analysis.

Data, Materials, and Software Availability. All study data are included in the article and/or *SI Appendix*.

Author affiliations: [a]Department of Plant Science, The Pennsylvania State University, University Park, PA 16802; [b]Centre for Crop Systems Analysis, Wageningen University and Research, Wageningen 6708PE, The Netherlands; [c]Department of Agronomy, University of Wisconsin, Madison, WI 53706; [d]Wisconsin Crop Innovation Center, University of Wisconsin, Madison, WI 53562; [e]Department of Biology, Faculty of Science, Mahidol University, Bangkok 10400, Thailand; [f]Future Food Beacon and School of Biosciences, University of Nottingham, LE12 5RD Nottingham, UK; and [g]School of Veterinary Medicine and Science, University of Nottingham, LE12 5RD Nottingham, UK

1. P. Grassini, K. M. Eskridge, K. G. Cassman, Distinguishing between yield advances and yield plateaus in historical crop production trends. *Nat. Commun.* **4**, 2918 (2013).
2. J. P. Lynch, Roots of the second green revolution. *Aust. J. Bot.* **55**, 493–512 (2007).
3. M. A. Sutton *et al.*, Too much of a good thing. *Nature* **472**, 159–161 (2011).
4. J. Lynch, Root phenotypes for improved nutrient capture: An underexploited opportunity for global agriculture. *New Phytologist* **223**, 548–564 (2019).
5. J. P. Lynch, Root phenes for enhanced soil exploration and phosphorus acquisition: Tools for future crops. *Plant Physiol.* **156**, 1041–1049 (2011).
6. R. Pieruschka, H. Poorter, Phenotyping plants: Genes, phenes and machines. *Funct. Plant Biol.* **39**, 813–820 (2012).
7. L. M. York, E. A. Nord, J. P. Lynch, Integration of root phenes for soil resource acquisition Integration of root phenes for soil resource acquisition. *Front. Plant Sci.* **4**, 355 (2013).
8. J. P. Lynch, Steep, cheap and deep: An ideotype to optimize water and N acquisition by maize root systems. *Ann. Bot.* **112**, 347–357 (2013).
9. J. P. Lynch, Root phenotypes for improved nutrient capture: An underexploited opportunity for global agriculture. *New Phytologist* **223**, 548–564 (2019).
10. J. P. Lynch, Root architecture and plant productivity. *Plant Physiol.* **109**, 7–13 (1995).
11. B. Hirel, J. Le Gouis, B. Ney, A. Gallais, The challenge of improving nitrogen use efficiency in crop plants: Towards a more central role for genetic variability and quantitative genetics within integrated approaches. *J. Exp. Bot.* **58**, 2369–2387 (2007).
12. J. P. Lynch, K. M. Brown, New roots for agriculture: Exploiting the root phenome. *Philos. Trans. R. Soc. Series B* **367**, 1598–1604 (2012).
13. J. P. Lynch, T. Wojciechowski, Opportunities and challenges in the subsoil: Pathways to deeper rooted crops. *J. Exp. Bot.* **66**, 2199–2210 (2015).
14. J. P. Lynch *et al.*, Root anatomy and soil resource capture. *Plant Soil.* **466**, 21–63 (2021).
15. J. A. Postma, J. P. Lynch, Root cortical aerenchyma enhances the growth of maize on soils with suboptimal availability of nitrogen, phosphorus, and potassium. *Plant Physiol.* **156**, 1190–1201 (2011).
16. J. P. Lynch, Root phenes that reduce the metabolic costs of soil exploration: Opportunities for 21st century agriculture. *Plant Cell Environ.* **38**, 1775–1784 (2015).
17. J. P. Lynch, Rightsizing root phenotypes for drought resistance. *J. Exp. Bot.* **69**, 3279–3292 (2018).
18. J. G. Chimungu, K. M. Brown, J. P. Lynch, Large root cortical cell size improves drought tolerance in maize. *Plant Physiol.* **166**, 2166–2178 (2014).
19. J. G. Chimungu, K. M. Brown, J. P. Lynch, Reduced root cortical cell file number improves drought tolerance in maize. *Plant Physiol.* **166**, 1943–1955 (2014).
20. H. Schneider *et al.*, Root cortical senescence decreases root respiration, nutrient content, and radial water and nutrient transport in barley. *Plant Cell Environ.* **40**, 1392–1408 (2017).
21. H. M. Schneider, J. P. Lynch, Functional implications of root cortical senescence for soil resource capture. *Plant Soil.* **423**, 13–26 (2017).
22. H. Schneider *et al.*, Root cortical senescence improves growth under suboptimal availability of N, P, and K. *Plant Physiol.* **174**, 2333–2347 (2017).
23. C. F. Strock, L. Morrow de la Riva, J. Lynch, Reduction in root secondary growth as a strategy for phosphorus acquisition. *Plant Physiol.* **176**, 691–703 (2018).
24. M. C. Drew, C. J. He, P. W. Morgan, Programmed cell death and aerenchyma formation in roots. *Trends Plant Sci.* **5**, 123–127 (2000).
25. J. Zhu, K. M. Brown, J. P. Lynch, Root cortical aerenchyma improves the drought tolerance of maize (Zea mays L.). *Plant Cell Environ.* **33**, 740–749 (2010).
26. J. A. Postma, J. P. Lynch, Theoretical evidence for the functional benefit of root cortical aerenchyma in soils with low phosphorus availability. *Ann. Bot.* **107**, 829–841 (2011).
27. P. Saengwilai, E. A. Nord, J. G. Chimungu, K. M. Brown, J. P. Lynch, Root cortical aerenchyma enhances nitrogen acquisition from low-nitrogen soils in maize. *Plant Physiol.* **166**, 726–735 (2014).
28. J. Chimungu *et al.*, Utility of root cortical aerenchyma under water limited conditions in tropical maize (Zea mays L.). *Field Crops Res.* **171**, 86–98 (2015).
29. T. Galindo-Castañeda, K. M. Brown, J. P. Lynch, Reduced root cortical burden improves growth and grain yield under low phosphorus availability in maize. *Plant Cell Environ.* **41**, 1579–1592 (2018).
30. R. E. Jaramillo, E. A. Nord, J. G. Chimungu, K. M. Brown, J. P. Lynch, Root cortical burden influences drought tolerance in maize. *Ann. Bot.* **112**, 429–437 (2013).
31. Y. Mano, F. Omori, Verification of QTL controlling root aerenchyma formation in a maize × teosinte "Zea nicaraguensis" advanced backcross population. *Breed Sci.* **58**, 217–223 (2008).
32. Y. Mano *et al.*, QTL mapping of root aerenchyma formation in seedlings of a maize × rare teosinte "Zea nicaraguensis" cross. *Plant Soil.* **295**, 103–113 (2007).
33. A. L. Burton *et al.*, QTL mapping and phenotypic variation of root anatomical traits in maize (Zea mays L.). *Theor. Appl. Genet.* **128**, 93–106 (2014).
34. H. Schneider *et al.*, Genetic control of root anatomical plasticity in maize. *Plant Genome* **13**, e20003 (2020).

35. S. Trachsel, S. M. Kaeppler, K. M. Brown, J. P. Lynch, Shovelomics: High throughput phenotyping of maize (Zea mays L.) root architecture in the field. *Plant Soil.* **341**, 75–87 (2011).

36. B. Hall, A. Lanba, J. Lynch, Three-dimensional analysis of biological systems via a novel laser ablation technique. *J. Laser Appl.* **31**, 022602 (2019).

37. C. F. Strock et al., Laser ablation tomography for visualization of root colonization by edaphic organisms. *J. Exp. Bot.* **70**, 5327–5342 (2019).

38. A. L. Burton, M. Williams, J. P. Lynch, K. M. Brown, RootScan: Software for high-throughput analysis of root anatomical traits. *Plant Soil.* **357**, 189–203 (2012).

39. C. F. Strock, H. M. Schneider, J. P. Lynch, Anatomics: High-throughput phenotyping of plant anatomy. *Trends Plant Sci.* **27**, 520–523 (2022).

40. S. C. Stelpflug et al., An expanded maize gene expression atlas based on RNA-sequencing and its use to explore root development. *Plant Genome* **9**, 314–362 (2015).

41. R. S. Sekhon et al., Genome-wide atlas of transcription during maize development. *Plant J.* **66**, 553–563 (2011).

42. M. Fan, R. Bai, X. Zhao, J. Zhang, Aerenchyma formed under phosphorus deficiency contributes to the reduced root hydraulic conductivity in maize roots. *J. Integr. Plant Biol.* **49**, 598–604 (2007).

43. F. Maniou, S. N. Chorianopoulou, D. L. Bouranis, New insights into trophic aerenchyma formation strategy in maize (Zea mays L.) organs during sulfate deprivation. *Front. Plant Sci.* **5**, 1–12 (2014).

44. H. Schneider, Characterization, costs, cues, and future perspectives of phenotypic plasticity. *Ann. Bot.* **130**, 131–148 (2022).

45. N. Niu et al., EAT1 promotes tapetal cell death by regulating aspartic proteases during male reproductive development in rice. *Nat. Commun.* **4**, 1445 (2013).

46. P. Muller, M. Ahmad, Light-activated cryptochrome reacts with molecular oxygen to form a flavin – superoxide radical pair consistent with magnetoreception. *J. Biol. Chem.* **286**, 21033–21040 (2011).

47. L. Consentino et al., Blue-light dependent reactive oxygen species formation by Arabidopsis cryptochrome may define a novel evolutionarily conserved signaling mechanism. *New Phytologist* **206**, 1450–1462 (2015).

48. A. Gunawardena, D. M. Pearce, M. B. Jackson, C. R. Hawes, D. E. Evans, Characterisation of programmed cell death during aerenchyma formation induced by ethylene or hypoxia in roots of maize (Zea mays L.). *Planta* **212**, 205–214 (2001).

49. D. E. Evans, Aerenchyma formation. *New Phytologist* **161**, 35–49 (2003).

50. A. M. Manschadi, J. Christopher, P. deVoil, G. L. Hammer, The role of root architectural traits in adaptation of wheat to water-limited environments. *Funct. Plant Biol.* **33**, 823 (2006).

51. V. R. P. Gowda, A. Henry, A. Yamauchi, H. E. Shashidhar, R. Serraj, Root biology and genetic improvement for drought avoidance in rice. *Field Crops Res.* **122**, 1–13 (2011).

52. A. Henry, V. R. P. Gowda, R. O. Torres, K. L. Mcnally, R. Serraj, Variation in root system architecture and drought response in rice (Oryza sativa): Phenotyping of the OryzaSNP panel in rainfed lowland fields. *Field Crops Res.* **120**, 205–214 (2011).

53. S. P. Klein, H. M. Schneider, A. C. Perkins, K. M. Brown, J. P. Lynch, Multiple integrated root phenotypes are associated with improved drought tolerance in maize. *Plant Physiol.* **183**, 1011–1025 (2020).

54. J. T. Yang, H. M. Schneider, K. M. Brown, J. P. Lynch, Genotypic variation and nitrogen stress effects on root anatomy in maize are node specific. *J. Exp. Bot.* **70**, 5311–5325 (2019).

55. H. M. Schneider et al., Root angle in maize influences nitrogen capture and is regulated by calcineurin B-like protein (CBL)-interacting serine/threonine-protein kinase 15 (ZmCIPK15). *Plant Cell Environ.* **45**, 837–853 (2022).

56. C. C. Subbaiah, M. M. Sachs, Molecular and cellular adaptations of maize to flooding ftress. *Ann. Bot.* **90**, 119–127 (2003).

57. I. Rajhi et al., Identification of genes expressed in maize root cortical cells during lysigenous aerenchyma formation using laser microdissection and microarray analyses. *New Phytologist* **190**, 351–368 (2011).

58. H. Takahashi, T. Yamauchi, I. Rajhi, N. K. Nishizawa, M. Nakazono, Transcript profiles in cortical cells of maize primary root during ethylene-induced lysigenous aerenchyma formation under aerobic conditions. *Ann. Bot.* **115**, 1–16 (2015).

59. A. I. Malik, T. D. Colmer, H. Lambers, M. Schortemeyer, Aerenchyma formation and radial O 2 loss along adventitious roots of wheat with only the apical root portion exposed to O 2 deficiency. *Plant, Cell & Environment* **26**, 1713–1722 (2003).

60. X. Zhang, G. Zhou, S. Shabala, A. Koutoulis, Identification of aerenchyma formation - related QTL in barley that can be effective in breeding for waterlogging tolerance. *Theor. Appl. Genetics* **129**, 1167–1177 (2016).

61. A. Promkhambut, A. Polthanee, C. Akkasaeng, A. Younger, Growth, yield and aerenchyma formation of sweet and multipurpose sorghum (Sorghum bicolor L. Moench) as affected by flooding at different growth stages. *Aust. J. Crop Sci.* **5**, 954–965 (2011).

62. E. Q. P. Tavares et al., The control of endopolygalacturonase expression by the sugarcane RAV transcription factor during aerenchyma formation. *J. Exp. Bot.* **70**, 497–506 (2019).

63. S. Jaffuel et al., Anatomical features of an African sorghum landrace adapted to flooded conditions. *Aust. J. Crop Sci.* **10**, 1489–1495 (2016).

64. S. Passot et al., Characterization of pearl millet root architecture and anatomy reveals three types of lateral roots. *Front. Plant Sci.* **7**, 1–11 (2016).

65. Y. Pan, Y. Xie, F. Li, B. Pan, Morphological and physiological responses to burial depth and sediment type in the wetland macrophyte Miscanthus sacchariflorus. *Fundam. Appl. Limnol.* **180**, 271–277 (2012).

66. C. J. Lawrence, The maize genetics and genomics database. The community resource for access to diverse maize data. *Plant Physiol.* **138**, 55–58 (2005).

67. C. N. Hansey, J. M. Johnson, R. S. Sekhon, S. M. Kaeppler, N. de Leon, Genetic diversity of a maize association population with restricted phenology. *Crop Sci.* **51**, 704–715 (2011).

68. R Core Team, R: A language and environment for statistical computing (Version 3.3.1., R Foundation for Statistical Computing, Vienna, Austria, 2018).

69. F. de Mendiburu, M. Yaseen, agricolae, Statistical Procedures for Agricultural Research (Version 1.4.0., R Package, 2020).

70. A. Kuznetsova, P. Brockhoff, R. Christensen, lmerTest package: Tests in linear mixed effects models. *J. Stat. Softw.* **82**, 1548–7660 (2017).

71. W. R. Fehr, *Principle of Cultivars Development* (Theory and Technique Macmillan Publishing, 1987).

72. D. Bates, M. Machler, B. Bolker, S. Walker, Fitting linear mixed-effects models using {lme4}. *J. Stat. Softw.* **67**, 1–48 (2015).

73. C. N. Hirsch et al., Insights into the maize pan-genome and pan-transcriptome. *Plant Cell* **26**, 121–135 (2014).

74. A. E. Lipka et al., GAPIT: Genome association and prediction integrated tool. *Bioinformatics* **28**, 2397–2399 (2012).

75. X. Gao, J. Starmer, E. R. Martin, A multiple testing correction method for genetic association studies using correlated single nucleotide polymorphisms. *Geneic Epidemiol.* **32**, 361–369 (2008).

76. R. C. Gentleman et al., Bioconductor: open software development for computational biology and bioinformatics. *Genome Biology* **5**, R80 (2004). https://doi.org/10.1186/gb-2004-5-10-r80.

77. B. Usadel et al., A guide to using MapMan to visualize and compare Omics data in plants: A case study in the crop species, Maize. *Plant Cell Environ.* **32**, 1211–1229 (2009).

78. J. L. Portwood et al., MaizeGDB 2018: The maize multi-genome genetics and genomics database. *Nucleic Acids Res.* **47**, 1146–1154 (2019).

79. Y. Jiao et al., Improved maize reference genome with single-molecule technologies. *Nature* **546**, 524–527 (2017).

80. M. Van Bel, PLAZA 4.0: An integrative resource for functional, evolutionary and comparative plant genomics. *Nucleic Acids Res.* **46**, D1190–D1196 (2018).

81. R. C. Edgar, MUSCLE: Multiple sequence alignment with high accuracy and high throughput. *Nucleic Acids Res.* **32**, 1792–1797 (2004).

82. M. N. Price, P. S. Dehal, A. P. Arkin, Fasttree: Computing large minimum evolution trees with profiles instead of a distance matrix. *Mol. Biol. Evol.* **26**, 1641–1650 (2009).

83. I. Letunic, P. Bork, Interactive tree of life (iTOL) v5: An online tool for phylogenetic tree display and annotation. *Nucleic Acids Res.* **49**, W293–W296 (2021).

84. D. R. McCarty et al., Steady-state transposon mutagenesis in inbred maize. *Plant J.* **44**, 52–61 (2005).

85. D. G. J. Mann et al., Gateway-compatible vectors for high-throughput gene functional analysis in switchgrass (Panicum virgatum L.) and other monocot species. *Plant Biotechnol. J.* **10**, 226–236 (2012).

86. A. H. Christensen, P. H. Quail, Ubiquitin promoter-based vectors for high-level expression of selectable and/or screenable marker genes in monocotyledonous plants. *Transgenic Res.* **5**, 213–218 (1996).

87. K. W. Earley et al., Gateway-compatible vectors for plant functional genomics and proteomics. *Plant J.* **45**, 616–629 (2006).

88. M. D. Curtis, U. Grossniklaus, A gateway cloning vector set for high-throughput functional analysis of genes in planta. *Plant Physiol.* **133**, 462–469 (2003).

89. D. McElroy, A. D. Blowers, B. Jenes, R. Wu, Construction of expression vectors based on the rice actin 1 (Act1) 5′ region for use in monocot transformation. *MGG Mol. General Genetics* **231**, 150–160 (1991).

90. N. O. Alieva et al., Diversity and evolution of coral fluorescent proteins. *PLoS One* **3**, e2680 (2008).

91. D. G. J. Mann et al., Switchgrass (Panicum virgatum L.) polyubiquitin gene (PvUbi1 and PvUbi2) promoters for use in plant transformation. *BMC Biotechnol.* **11**, 74 (2011).

92. T. Čermák et al., A multipurpose toolkit to enable advanced genome engineering in plants. *Plant Cell* **29**, 1196–1217 (2017).

93. L. Stavolone, A. Ragozzino, T. Hohn, Characterization of Cestrum yellow leaf curling virus: A new member of the family Caulimoviridae. *J. General Virol.* **84**, 3459–3464 (2003).

94. B. Frame, M. Main, R. Schick, K. Wang, "Genetic transformation using maize immature Zygotic Embryos" in *Plant Embryo Culture: Methods and Protocols*, T. Thorpe, E. Yeung, Eds. (Humana Press, Totowa, NJ, 2011), pp. 327–341.

95. B. A. Lowe et al., Marker assisted breeding for transformability in maize. *Mol. Breeding* **18**, 229–239 (2006).

96. H. J. Kim, H. J. Lee, H. Kim, S. W. Cho, J. S. Kim, Targeted genome editing in human cells with zinc finger nucleases constructed via modular assembly. *Genome Res.* **19**, 1279–1288 (2009).